

CHAPTER 2 REVIEW OF RELEVANT STUDIES

2.1 Introduction

Knee-braced Moment Frames (KBMFs) are a structural system that combines the salient features of moment resisting frames and eccentrically braced frames. The system uses moment resisting frames together with stocky knee braces as the means to resist seismic forces. KBMF structural system is designed based on capacity design concept that results in a ductile seismic behavior. After a moderate earthquake, these frames can be easily repaired by replacing the knee braces [1].

In this study, an improved version of the KBMF system is presented and called Knee-braced moment frame with Partially-restrained Connections (KBMF with PR Connections). Partially restrained (PR) connections are used. For this study, bolted top and seat angle connections with double web angles were used. During the past decade, many studies involving the feasibility of using bolted top and seat angle connections with double web angles have been carried out. These connections are designed based on actual behavior of joints which need in understanding the moment-rotation behavior of connections. In addition to the use of PR connections, two different types of knee braces were considered in this study, regular buckling braces and buckling-restrained braces (BRBs). Relevant research results are presented in the following sections.

2.2 Knee-Braced Moment Frames

2.2.1 Design Concept

KBMF is designed based on capacity design concept that results in a ductile seismic behavior. The design concept of KBMFs is based on a predetermined yield mechanism that limits elastic activities to ductile segments of the frame. For this system, the frames can be designed such that the knee braces yield and buckle under seismic loads followed by plastic hinging of beam at the end of the beam outside the knee portions. The seismic energy is dissipated by a mean of this yield mechanism. The strength of the knee braces is selected so as to achieve the wanted mechanism.

Figures 2.1 and 2.2 show the yield mechanism of KBMF and equilibrium of forces in the knee region, respectively. Based on plastic design concept, the strength of the knee braces required to complete the selected mechanism has been obtained by Leelataviwat et al. [1]. In this mechanism, moment of the beam-to-column connections is kept to a value below the yield moment to reduce the possibility of the connection failure. Other members in the frame are designed as elastic under the largest forces generated by fully yielded and strain-hardened plastic hinge and knee braces except at the column bases where plastic hinges are required to complete the mechanism.

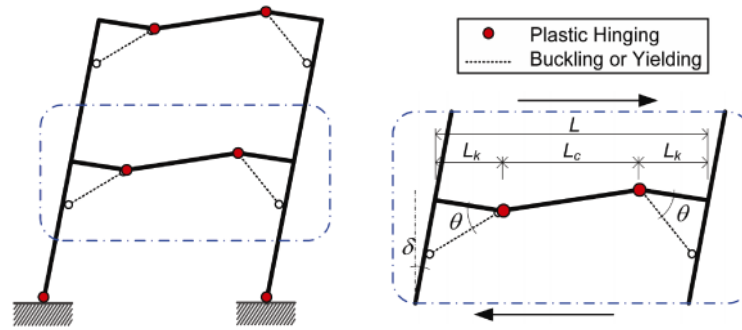


Figure 2.1 Yield Mechanism of KBMF System [1].

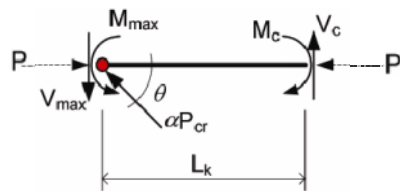


Figure 2.2 Equilibrium of Forces in Knee Region of KBMF [1].

In designing a KBMF, The first step is the design of the base moment frame. After the base moment frame has been designed, the knee braced can be sized under the selected yield mechanism. For the first approximation, gravity loads can be considered small and can be neglected. From Figure 2.2, the moment at the beam-to-column connection can be expressed as:

$$M = M_{\max} + V_{\max} L_k - \alpha P_{cr} \sin(\theta) L_k \quad (2.1)$$

The maximum moment at the connection occurs when the beam reaches M_{\max} , and the knee brace reaches the final post-buckling strength (P_{cr}). In this case the fully yielded and strain hardened plastic moment of the beam can be estimated by multiplying the plastic moment by the overstrength factor:

$$M_{\max} = \xi M_p \quad (2.2)$$

The maximum shear force that can be developed is related to the maximum moment:

$$V_{\max} = \frac{2M_{\max}}{L_c} \text{ or } \frac{2\xi M_p}{L_c} \quad (2.3)$$

where M_{\max} and V_{\max} are the maximum moment and the maximum shear force, ξ is the post-buckling strength reduction, P_{cr} is the buckling strength of the knee braces, θ is the angle between the knee braced and the beam, and L_k is the length of the knee portion, M_p is the plastic moment of the beam and L_c is the length of the clear span.

The moment at the beam-to-column connection given by Equation 2.1 can be limited by the plastic moment of the beam not to exceed an acceptable level, that is:

$$M \leq \gamma M_p \quad (2.4)$$

where γ is a numerical factor with a value less than 1.0. This factor can be chosen depending on the allowable moment at the connection. By using Equations 2.2 through 2.4, Equation 2.1 can be calculated in a dimensionless form as follows:

$$\frac{\alpha P_{cr}}{M_p / L} \geq \frac{(\xi - \gamma)}{(L_k / L) \sin(\theta)} + \frac{2\xi}{(1 - 2L_k / L) \sin(\theta)} \quad (2.5)$$

The above equation can be used for calculating the post-buckling strength of the knee brace. The key functions of the equation are to limit the moment at the connection and to allow the frame complete the selected mechanism. By using this equation, the size of the knee brace can be determined when the length of the knee portion, the angle of the knee brace, and the size of the beam are selected.

The overstrength factor, ξ in Equation 2.5 was calculated using formula which proposed by Boonpao et al. The overstrength factor of the beam can be expressed as:

$$\xi = 1 + \left[\frac{\left(\frac{\beta \times 6EI}{L_c} \right) \left[(\theta_p) \left(1 + \frac{2L_k}{L_c} \right) \right]}{M_p} \right] \quad (2.6)$$

where θ_p is the plastic story drift of the frame and β is the post-yield stiffness factor of the beam.

2.2.2 Dynamic Response of KBMFs

Recently, the dynamic behavior of an example KBMF was investigated by Srechai [21]. Response of KBMFs designed by various different methods under nonlinear static analysis (Pushover) and nonlinear dynamic analysis were compared with the response of a conventional moment resisting frame (MRF). A three-story building was selected to study the seismic response of both frames. The totals of four design cases for the three story building frames were conducted.

In the study, an analytical model of KBMF was developed to study the dynamic behavior. The model was calibrated with test results to accurately capture the nonlinear behavior of KBMFs. A finite-element based computer code was employed to simulate cyclic behavior of the frame. The model considers three main components such as knee braces, beams and columns, and panel zones. The knee-braces, beams, and columns in the frame were model using the axial compression element and beam-column elements from the program, respectively. The shear resistance of the panel zone was simulated by two rotation springs representing the column web and the column flange, respectively. The hysteretic response from the simulation comparing with test result was shown in

Figure 2.3. It was found that an appropriate value for the strain-hardening was in the order of 8%.

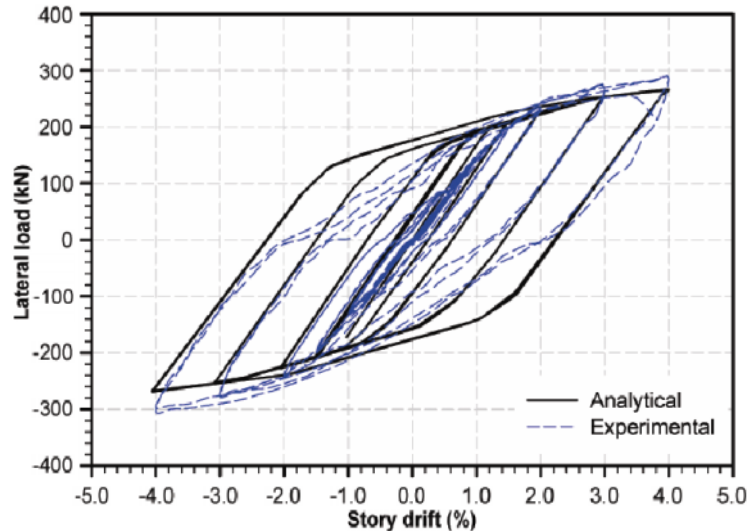


Figure 2.3 Simulation of Test Result by Sechai [21].

Three-story buildings were created to study the dynamic behavior. Nonlinear static (Pushover) and nonlinear dynamic analyses were employed. A total of four design cases for the three story building frame were conducted. The frame was designed based on the IBC-2000 provisions. Important constants used to calculate the design spectrum were $S_1 = 0.8g$ and $S_2 = 1.2g$, Seismic Use Group I, and Soil Type B.

The first three cases utilized the conventional design method in which the design forces were derived from the elastic analysis reduced by a constant response reduction factor. In the first case, the frame was designed as a conventional MRF using $R=8$. This case served as the base line for comparison. In the second case, the frame was designed with $R=8$ and the knee braces were added into the frame to make it a KBMF. The braces were designed based on capacity design concept presented by Leelataviwat et al. [1] using the L_k/L ratio of 0.2. In the third case, the moment frame in the KBMF was first designed using the design base shear of 0.7 times the design base shear calculated using $R=8$. The knee braces were then additionally designed by the same method used in the second case.

The fourth case utilized a performance-based plastic design (PBPD) approach [18] that explicitly considered the yield strength, yield mechanism and target displacement. The KBMF in this case was designed using the same seismic design factors as the three frames described before. The maximum target drift was selected as 2.0 percent at the design basis earthquake level with an assumed yield drift of 1.0 percent. The estimated period, T , of the frame was 0.75 second. The design base shear coefficient (V/W) calculated by the PBPD procedures was 0.314. Figure 2.4 shows the results of four design cases of the three-story building frame.

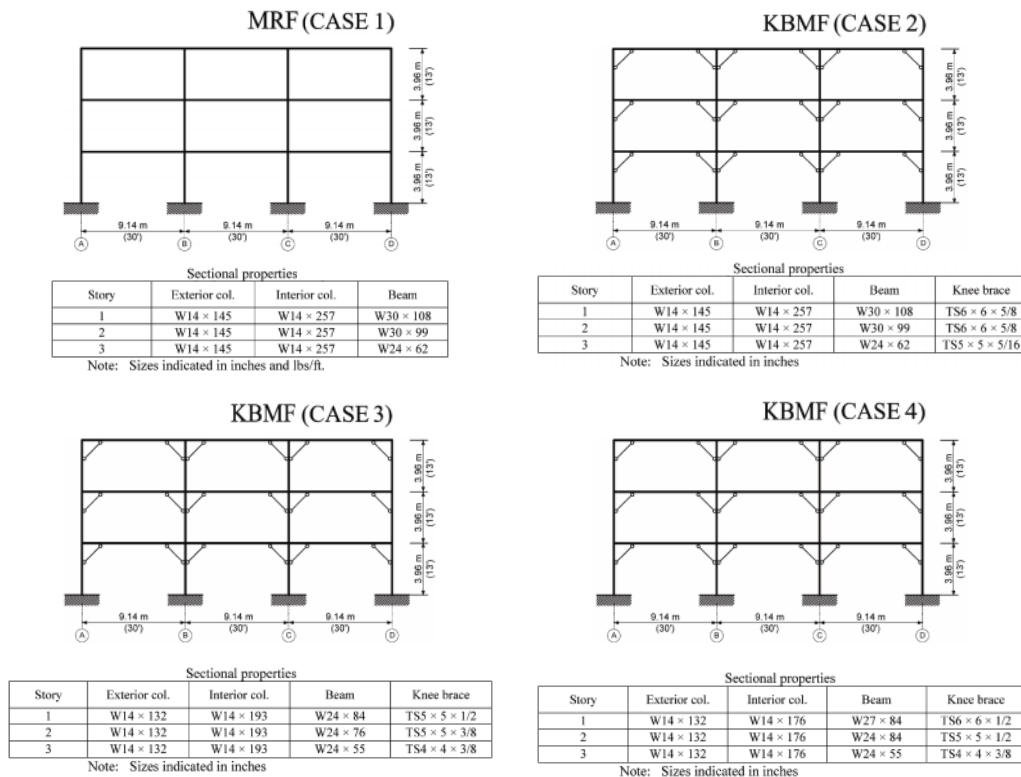


Figure 2.4 Four Cases of Three-Story Building Frame used by Srechai [21].

The plots of the base shear versus roof drift of the four frames are shown in Figure 2.5. The KBMFs provide superior seismic performance than the MRF frame. For the same system strength, the stiffness of KBMFs is almost 20 percents larger than that of the MRF.

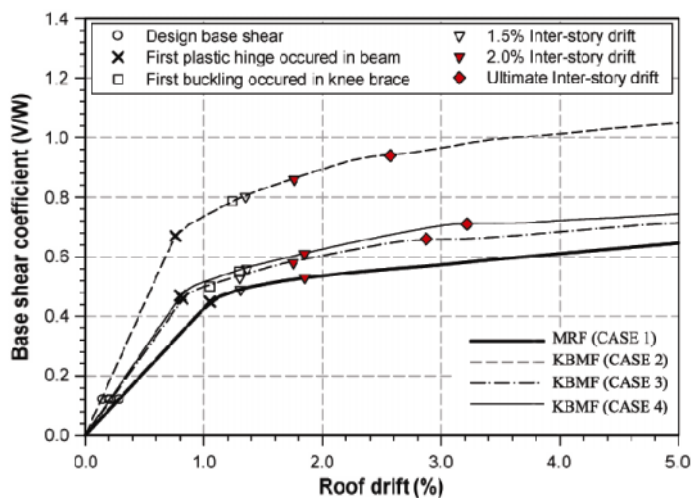


Figure 2.5 Base Shear Versus Roof Drift from NSA of MRF (CASE 1), KBMF (CASE 2), KBMF (CASE 5), and KBMF (CASE 4) from Srechai [21].

The comparison of average maximum inter-story drifts under DBE and MCE ground motions of three-story studies frame are shown in Figures 2.6 and 2.7, respectively. The inter-story drifts of KBMFs were less than that of the MRF frames by 10-40 percents. The results from this study show that KBMFs have a ductile behavior with all inelastic behavior confined only to the designated elements in the frame.

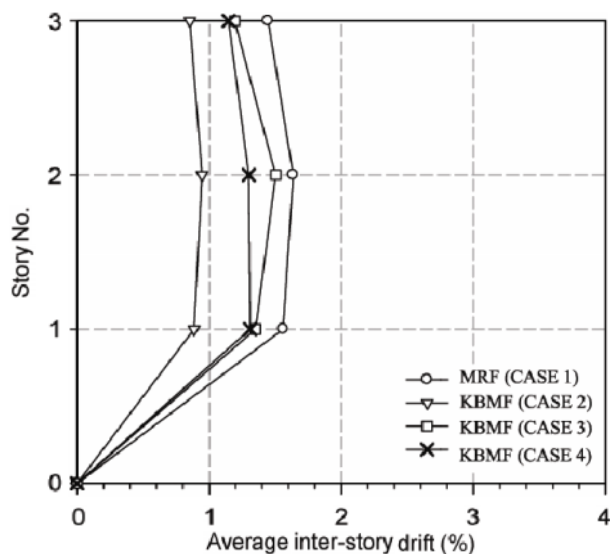


Figure 2.6 Average Maximum Inter-Story Drifts under DBE Ground Motions of Three-Story Study Frames [21].

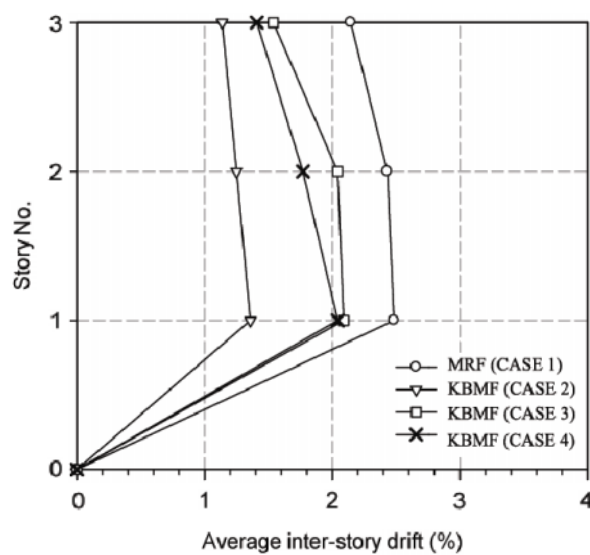


Figure 2.7 Average Maximum Inter-Story Drifts Under MCE Ground Motions of Three-Story Study Frames [21].

2.3 Partially Restrained (PR) Connections or Semi-rigid Connections

2.3.1 Introduction

The analysis and design of steel frames are typically performed under an assumption that the connections are either fully rigid or pinned. The assumption of a fully rigid connection implies that the connection can completely transfer the end moment out with any relative rotation, while the pinned connection assumes that free rotation of the connection is possible and the connection moment is zero [6,7]. On the other, all beam-to-column connections that act between the two extreme cases of fully rigid and pinned, are called partially restrained (PR) or semi-rigid connections.

Partially restrained or semi-rigid connections are classified as Type 3 connection, called “Semi-rigid Framing” in Allowable Stress Design (ASD) Specification [8] and “Type PR” (Partially Restrained) in Load and Resistance Design (LRFD) Specification [9]. In PR-type, the connections can transfer shear and some moment. The connection rotates when a moment is applied. The behavior of PR connections may be represented by moment-rotation relationship. The typical moment rotation curve of a PR connection is between the two extreme cases as shown in Figure 2.8.

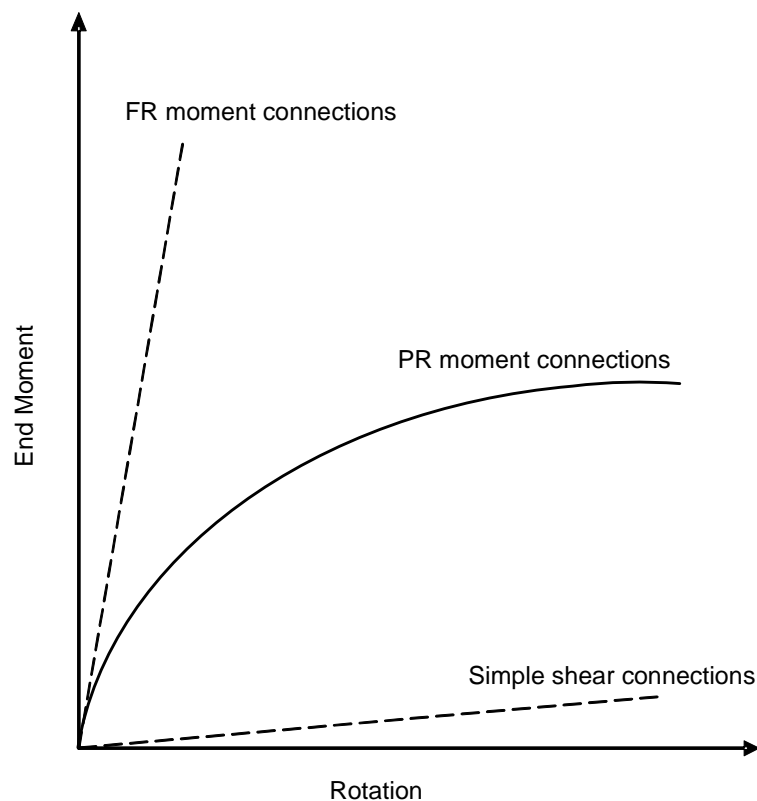


Figure 2.8 Moment-Rotation Curves of PR Connections.

Based on the AISC LRFD Specification, the connection is referred to as a partially restrained (PR) moment connection when the deformation of the connection elements affects the resistant of structure. For a frame with PR connections, the stiffness, strength, and ductility of the connection must be considered in the design [9].

A typical curve of a PR connections moment–rotation is shown in Figure 2.9. In terms of the connection stiffness, if $K_s L/EI \geq 20$. It is acceptable to consider the connection to be fully restrained (FR) connection. But $K_s L/EI \leq 2$, it is acceptable to consider the connection to be simple shear connection, where K_s is secant stiffness, L and EI are the length and the bending rigidity of the beam respectively, Connections with stiffness between these two limits are partially restrained (PR) connection.

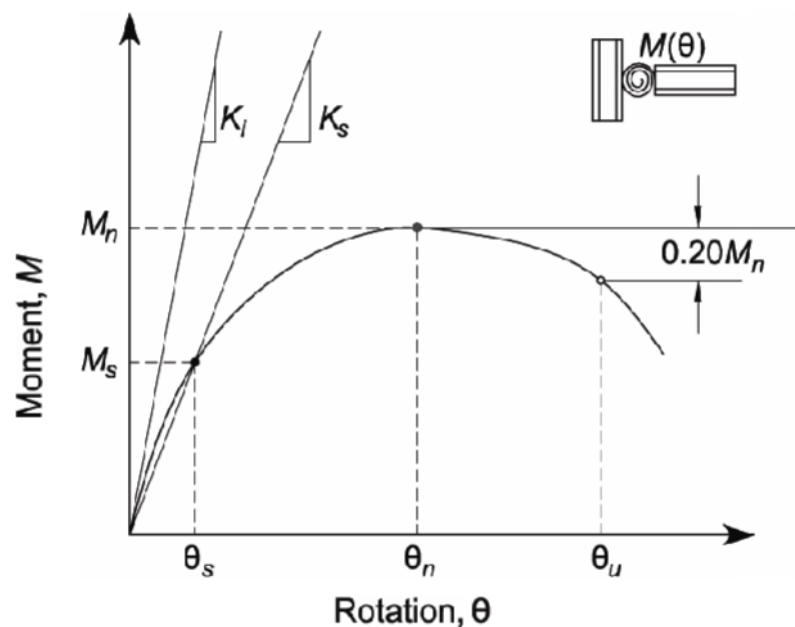


Figure 2.9 Definition of Stiffness, Strength and Ductility Characteristics of Moment-Rotation Response of a PR Connections [9].

2.3.2 Behavior of PR connections

Common PR connections include double-web angles, single tee, top and bottom angles, top and bottom tees, extended end plate, top and bottom plates with web connections, and top and bottom angles with double web angles connections [10]. The eight types of common PR connections are summarized by Dhillon et al. and are shown in Figure 2.10. Experiments have shown that, the flexibility of a connection depends on the geometric properties of the elements in the connection. The moment–rotation curves of these PR connections exhibit nonlinear behavior that depends on many factors such as yielding or buckling of some component, plate slipping, etc. The single web-angle connection represents a very flexible joint, and the T-stub connection represents a rather rigid connection. The moment-rotation curves of each type of connections are shown in Figure 2.11.

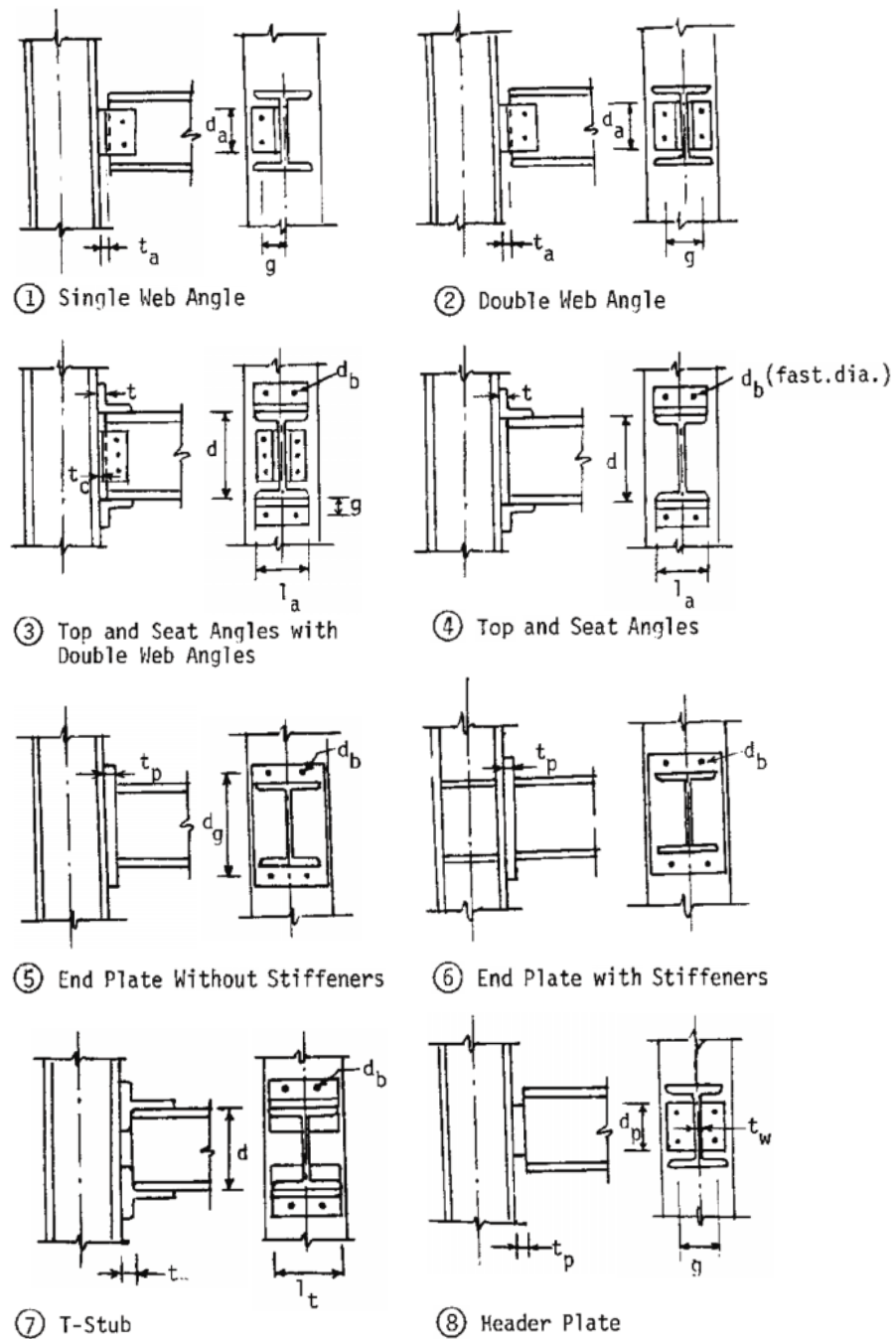


Figure 2.10 Typical Types of PR Connections as summarized by Dhillon et al. [10].

This research focuses on the top and seat bolted angle connections with double web angles. This type of connection combines the top and seat angle connections with double web angle. For this connection, double web angles are utilized to help top and seat angles in transferring the moment at the joint.

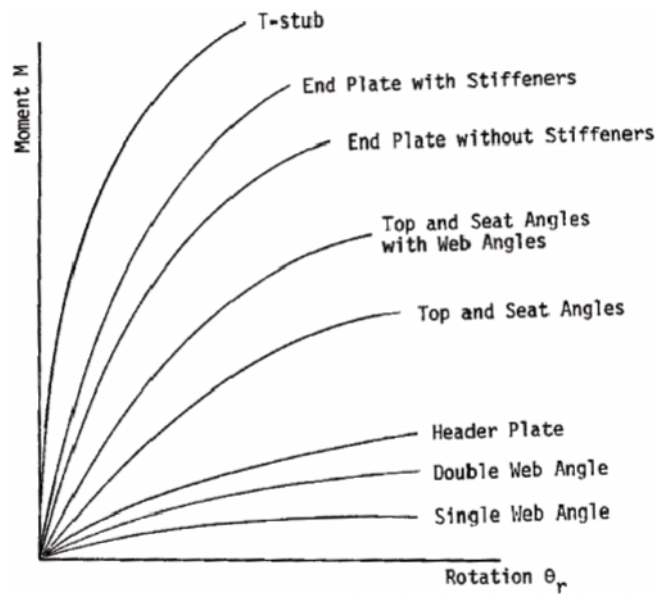


Figure 2.11 Typical Moment-Rotation Curves as presented by Dhillon et al. [10].

Calado et al. [4] carried out experimental studies the behavior of PR connections under monotonic and cyclic load. Three full-scale specimens were tested at the Material and Structures Test Laboratory in Lisbon. The overview of the test set-up is illustrated in Figure 2.12.

Tested specimens consisted of IPE300 beam section joined to three different column sizes (HEB160, HEB200, and HEB240). The top, seat, and web angles were connected by bolts. For angles, L section 120×120×10 was used for all cases. Top and seat angles were connected by 4M16 bolts arranged in two rows on column and beam flanges, while double web angles were connected by 3M16 bolts, arranged in one column on the beam web and column flange.

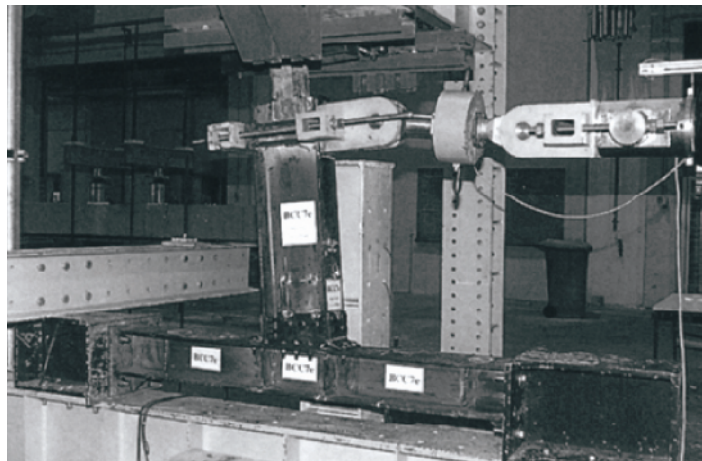


Figure 2.12 Overview of Example Tested Connection carried out by Calado et al. [4].

An example of the cyclic response of top and seat angle connections with double web angles is presented in Figure 2.13. The loops show a pinching behavior with a significant reduction of stiffness whenever rotation approaches zero. The behavior of the specimens is characterized by slippage, and contact and detachment behaviors that affect the inelastic response. The main cause of this pinching behavior is the development of the gap between top or seat angle and column flange during the tension loading stage as shown in Figure 2.14. However, increase in stiffness occurs again when the contact is formed between the angle and the column flange during compression loading.

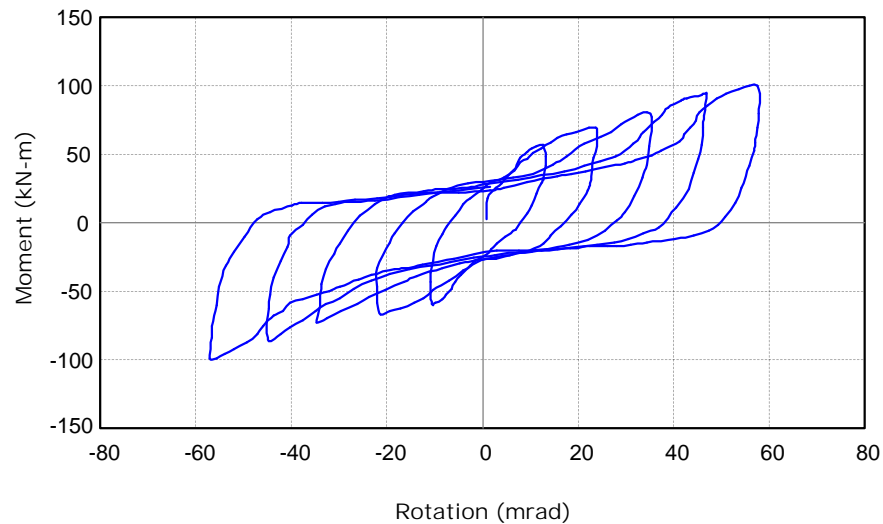


Figure 2.13 Moment-Rotation Hysteresis for Top and Seat Angle Connections with Double Web Angles obtained by Calado et al. [4].

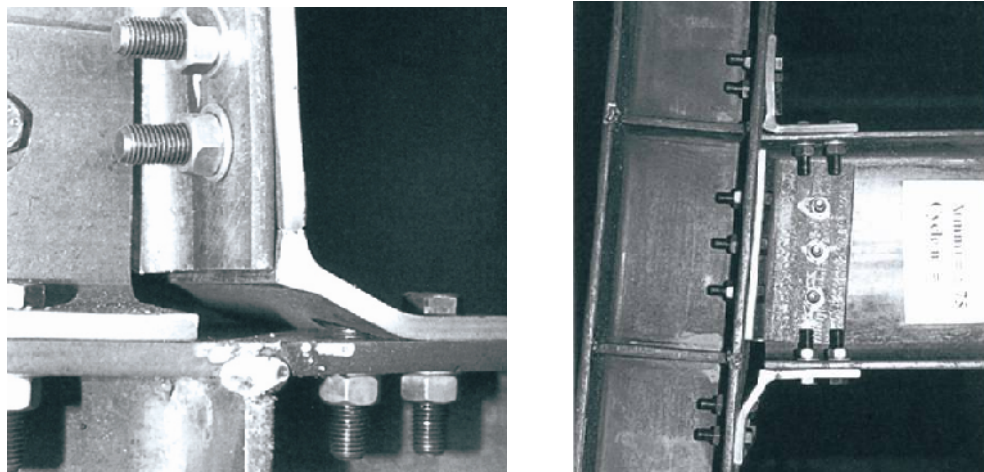


Figure 2.14 Development of a Gap at Column Flange as observed in the test carried out by Calado et al. [4].

2.4 Knee-braced Moment Frame with Partially-restrained Connection (KBMF with PR connections)

An improved version of the KBMF system is presented in this section. Partially restrained (PR) connections are used in connecting the beams to the columns in the KBMFs system that called Knee-braced Moment Frames with Partially-restrained connections (KBMFs with PR connections). A bolted top and seat angle connections with double web angles were used. The use of PR connections can eliminate the problem facing the repair of welded connections. Moreover, PR connections exhibit large ductility and energy dissipation capacity.

2.4.1 Cyclic Testing of KBMF with PR connections

The proposed KBMFs with PR connections represent a future generation of a high performance structural system. To study the behavior of this system, a prototype of frame specimen was fabricated and tested under cyclic loading. The frame was designed using the procedure described by Leelataviwat et al. [1]. The frame was designed assuming an overstrength factor, ξ , of 1.2 at 3% story drift. The allowable bending moment at the connection was selected to be 80% of the plastic moment of the beam ($\gamma = 0.80$). Three parameters power model [6,7] was employed to design the beam-to-column connections in the frame. The length of the knee portion has been chosen to be 20% of the span length ($L_k/L = 0.20$), which where the optimum values were suggested by Leelataviwat et al. [1].

The final design resulted in the KBMF with PR connections consisting of a 4 meters long W250×125-29.6 kg/m beam, 2 meters high W250×250-72.4 kg/m columns, and $\phi 76.2 \times 3.9$ knee braces. Table 2.1 shows the section properties of the frame. For the connection design, L150 × 150 × 13 mm top-and-seat angles were used to connect the beam flanges to the column flange with M22 bolts. Angles L100 × 100 × 13 mm double web angles were used to connect the beam web to the column flange with M16 bolts. 9 mm plates were used as a stiffener in the beam-to-column connections, beam, and column.

Table 2.1 Section Properties of Frame Test.

Member	Section	Steel Grade
Beams	H250 × 125-29.6 kg/m.	A36
Columns	H250 × 250-72.4 kg/m.	A36
Knee Braces	Circular tube 76.2 × 3.9	A36

The schematic of the test specimen is shown in Figure 2.15. The specimen was instrumented with strain gauges at key locations and painted with whitewash to facilitate the observation. The test was carried out at the Asian Institute of Technology. The specimen was subjected to cyclic loading with the loading history shown in Figure 2.16.

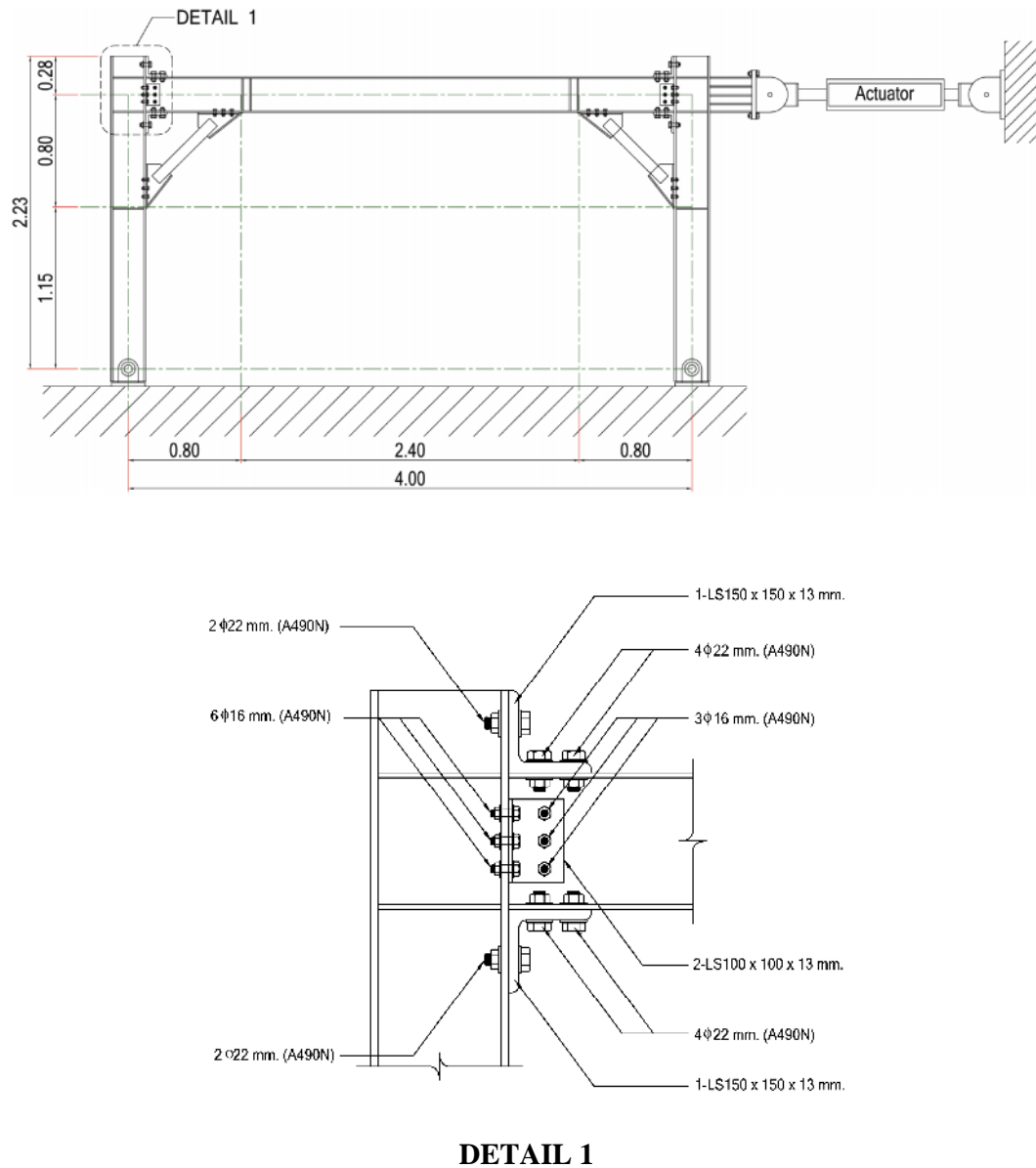


Figure 2.15 Schematic of Test Specimen.

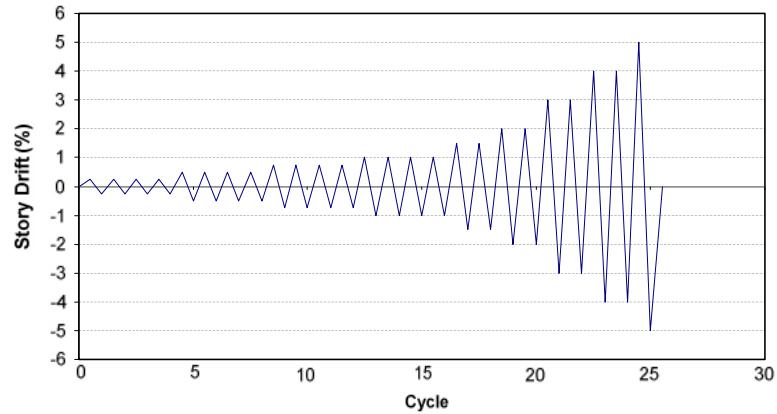


Figure 2.16 Loading History of KBMF Test Frame.

Figure 2.17 shows the hysteretic response of the KBMF with PR connections obtained from the test. The experimental result from cyclic testing showed a stable hysteretic characteristic response with pinching behavior.

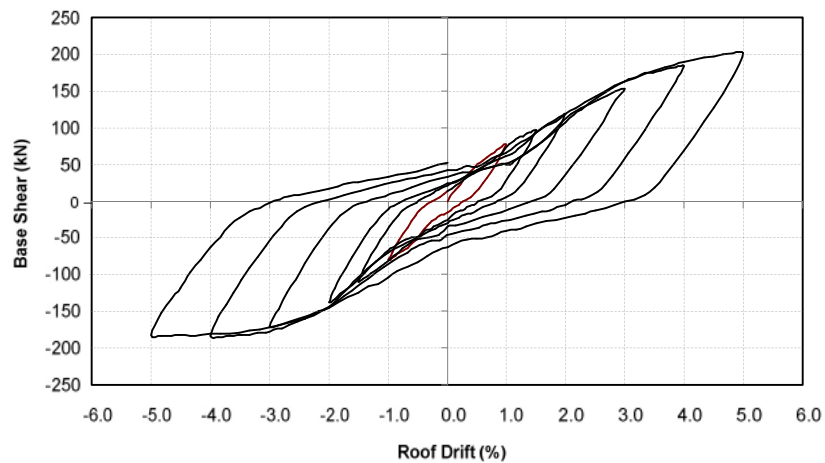


Figure 2.17 Hysteretic Loops of Test Result.

The hysteretic loops showed an apparent pinching behavior. The pinching may result from the combination of the opening and closing of gaps and slippage at bolt-holes in the PR connections and the braces. Figure 2.18 shows the gaps between outstanding of top angle and column flange. Moreover, in the later stage of loading cycles, local plastic deformation in the beam flange at the contact points between the beam and the ends of the braces was clearly evident as shown in Figure 2.19. The gaps and the bolt slippage affected the deformation of the knee braces and resulted in much smaller strain values in the braces that affected large pinching behavior in hysteretic loops.

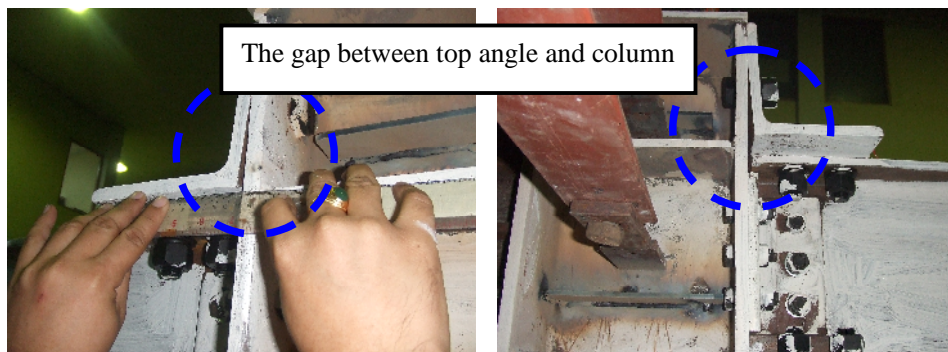


Figure 2.18 Opening of Gap between Column and Angle.

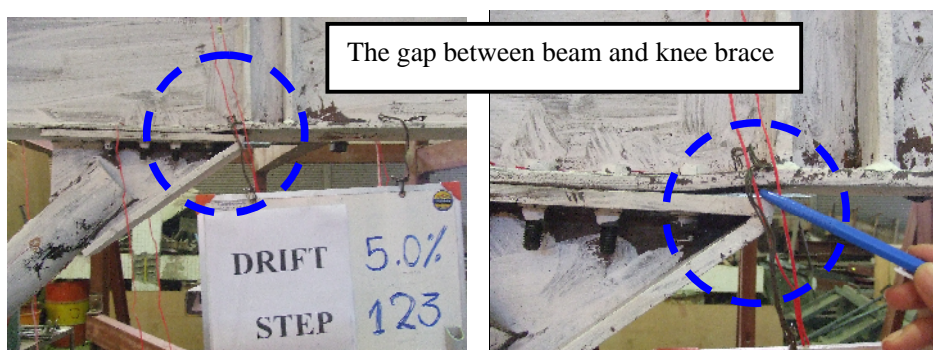


Figure 2.19 Gap between Beam and Knee Brace.

The specimen continued to carry the load up to the story drift of 5%. At this drift level, the mechanism could be clearly identified; axial yielding occurred in the knee braces and plastic hinge occurred in the beam, as shown in Figure 2.20.



Figure 2.20 Plastic Hinging and Brace Yielding in Test Specimen at 5% Story Drift.

2.5 Method for Predicting Rotational Behavior of PR Connections

Many methods for modeling the joints behavior have been developed and proposed by researchers [6,7,13,14]. The objectives of every method are to simulate the moment-rotation behavior for structural analysis purposes. In this study, selected mathematical representations of moment-rotation behavior and mechanical models are presented.

2.5.1 Mathematical representation of Moment-Rotation Curve

PR connections or Semi-rigid connections require certain moment-rotation curves for analysis and design processes. The overall of joint behavior can be represented by mathematical expressions such as linear, bilinear, multi-linear, and nonlinear equations.

One popular nonlinear expression is the three-parameter power model developed by Kishi and Chen [6]. This model simulates the $M-\theta$ curve using mathematical expressions that consider material and geometric properties. The main parameters of the model are the initial connection stiffness, the ultimate moment capacity of the connection, and the shape parameter. The model is suitable for representing of connection behavior, and can be applied in the second-order nonlinear frame analysis with PR connections [6,7]. The generalized form of this model is given by:

$$M = \frac{R_{ki}\theta_r}{\left[1 + \left(\frac{\theta_r}{\theta_0}\right)^n\right]^{1/n}} \quad (2.7)$$

where M is the end moment of a connection, R_{ki} is the initial stiffness parameter, θ_0 is the reference plastic rotation, and n is the shape parameter. The initial connection stiffness (R_{ki}) and the ultimate connection moment (M_u) can be determined from the equations below.

The initial stiffness of the top and seat angle with double web angles connection can be determined from combining the stiffness of the three main elements in the connection is:

$$R_{ki} = K_{it} + K_{is} + K_{ia} \quad (2.8)$$

where K_{it} , K_{is} , and K_{ia} are the initial stiffness contributed by the top angle, seat angle and web angle respectively.

For the ultimate moment capacity (M_u), the plastic mechanism moment of a connection is the summation of the plastic moment capacities contributed by the assembly angles. The plastic beam theory considering the moment-shear interaction is used to derive the expression for the mechanism moment [6,7]. The ultimate moment of the top and seat angle with double web angles connection is given by:

$$M_u = M_{os} + M_{pt} + V_{pt}d_2 + 2V_{pa}d_4 \quad (2.9)$$

where M_{os} is the plastic moment of the seat angle, M_{pt} is the plastic moment of the top angle, V_{pt} is the plastic shear force in vertical leg of the top angle, V_{pa} is the plastic shear force in a single web connection, d_2 is the distance from the center of rotation of the top angle to the line of the force V_{pt} , and d_4 is the distance from the center of rotation of the angle connection to the line of the force V_{pa} .

Finally, shape parameter (n) is determined by using the method of least squares approximation for the difference between the experimental and the predicted moment data [6]. Figure 2.21 shows the shape of the moment-rotation curves for different n values.

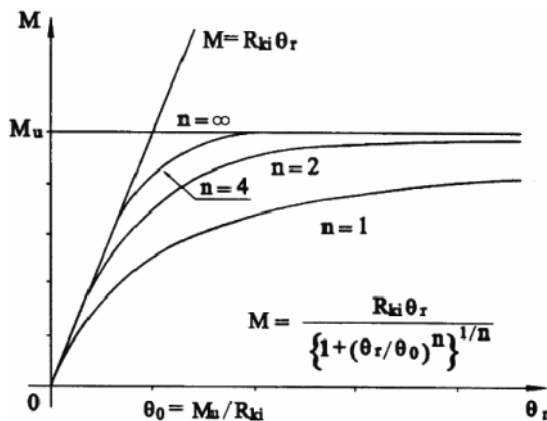


Figure 2.21 Curves of E-P-P Moment-Rotation Equation presented by Chen [6].

2.5.2 Moment-Rotation Behavior Models

Models for predicting the connection behavior can be classified into three different types, namely empirical, finite element, and mechanical models. Each model has to be combined with a mathematical representation of a moment-rotation curve. The following section summarizes the features of these models.

1. Empirical models

Empirical models use the empirical formulations involved in the mathematical representation of the moment-rotation considering the geometrical and mechanical properties of beam-to-column joints. These formulations are defined by data which can be obtained in different ways such as experimental testing, or parametric analyses developed by finite element models, analytical models or mechanical models. The first empirical model was developed by Frye and Morris [20] using odd-power polynomial representation of the moment-rotation curve. It can be shown that the rotation is given by:

$$\theta = C_1(KM) + C_2(KM)^3 + C_3(KM)^5 \quad (2.10)$$

where K depends on the geometrical and mechanical properties of the structural details, C_1 , C_2 , C_3 are curve-fitting constants shown in Table 2.2. The connection parameters correspond to the connection types are indicated in Figure 2.10 (page number of 12).

Table 2.2 Standardized Connection Constants summarized by Dhillon et al. [10].

Connection types	Curve-fitting constants	Standardization constant
Single web-angle	$C_1 = 4.28 \times 10^{-3}$ $C_2 = 1.45 \times 10^{-9}$ $C_3 = 1.51 \times 10^{-16}$	$K = d_a^{-2.4} t_a^{-1.81} g^{0.15}$
Double web-angle	$C_1 = 3.66 \times 10^{-4}$ $C_2 = 1.15 \times 10^{-6}$ $C_3 = 4.57 \times 10^{-8}$	$K = d_a^{-2.4} t_a^{-1.81} g^{0.15}$
Top and seat angle with double web angle	$C_1 = 2.23 \times 10^{-5}$ $C_2 = 1.85 \times 10^{-8}$ $C_3 = 3.19 \times 10^{-12}$	$K = d^{-1.287} t^{-1.128} t_c^{-0.415} l_a^{-0.694} g^{1.35}$
Top and seat angle	$C_1 = 8.46 \times 10^{-4}$ $C_2 = 1.01 \times 10^{-4}$ $C_3 = 1.24 \times 10^{-8}$	$K = d^{-1.5} t^{-0.5} l_a^{-0.7} d_b^{-1.5}$
End-plate with out column stiffener	$C_1 = 1.83 \times 10^{-3}$ $C_2 = 1.04 \times 10^{-4}$ $C_3 = 6.38 \times 10^{-6}$	$K = d_g^{-2.4} t_p^{-0.4} d_b^{-1.5}$
End-plate with column stiffeners	$C_1 = 1.79 \times 10^{-4}$ $C_2 = 1.76 \times 10^{-4}$ $C_3 = 2.04 \times 10^{-4}$	$K = d_g^{-2.4} t_p^{-0.6}$
T-stub	$C_1 = 2.10 \times 10^{-4}$ $C_2 = 6.20 \times 10^{-6}$ $C_3 = -7.60 \times 10^{-9}$	$K = d^{-1.5} t^{-0.5} l_t^{-0.7} d_b^{-1.1}$
Header-plate	$C_1 = 5.10 \times 10^{-5}$ $C_2 = 6.20 \times 10^{-10}$ $C_3 = 2.40 \times 10^{-13}$	$K = d_p^{-2.3} t_p^{-1.6} t_w^{-0.5} g^{1.6}$

2. Finite element models

Finite element analysis is one of the most suitable methods to investigate the response of a connection. The finite element technique is an accurate tool for modeling welded beam-to-column joints. Accurate finite element analysis of a bolted steel joint requires the modeling of geometrical and material nonlinearities of the elementary parts of the connection, interaction between bolts and plate components, slip due to bolt-to-hole clearance, variability of contact zones, etc. Using finite element analysis, the basic mechanisms of these interactions need to be fully understood. However, its application in modeling bolted connections is still largely unexplored. An example of bolted connection finite element model is shown in Figure 2.22. At this time, finite element analysis of bolted connections is primarily for research purposes.

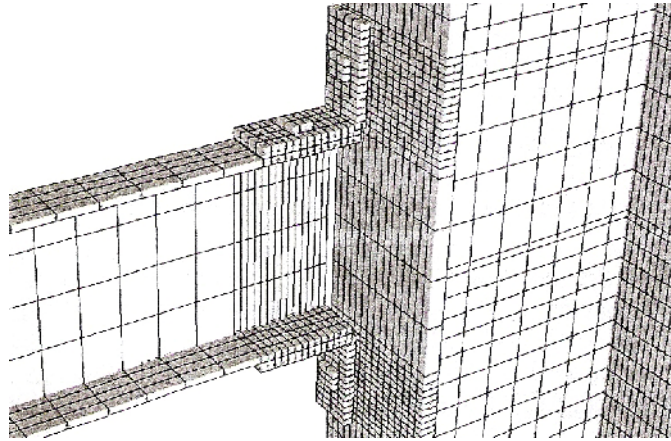


Figure 2.22 Finite Element Model used by Raffaele [11].

3. Mechanical Models

Mechanical models or spring models are based on the simulation of connecting elements using a set of rigid and deformable elements. The model is characterized by nonlinear springs and shear springs. The first type accounts for the deformation due to the tension or compression loads transmitted through the beam flange; the second type simulates the shear deformation of the panel zone [15]. Mechanical models are suitable for modeling the connections response providing that the knowledge of the stress-deformation relationship of the spring is available. These relationships can be obtained by experimental tests or analytical models. This type of model can be used to simulate monotonic and cyclic behavior. Figure 2.23 shows an example of a mechanical model for top and seat angle connections with web angles.

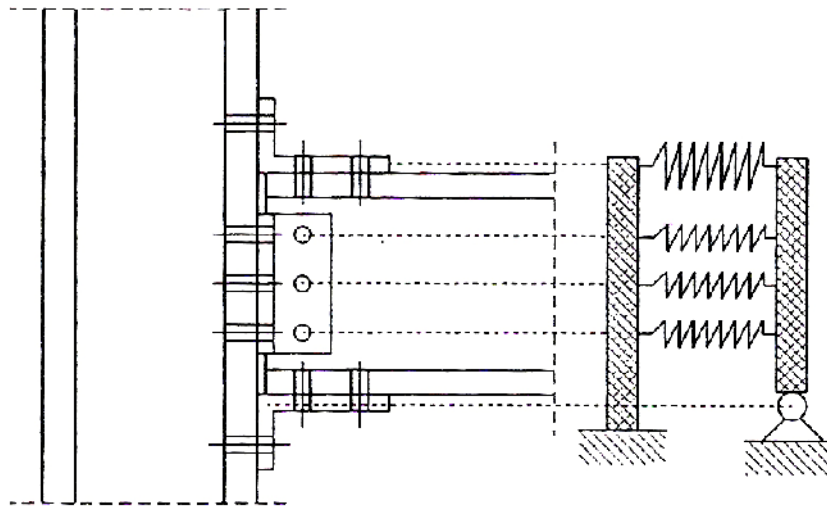


Figure 2.23 Mechanical Model for Top and Seat Angle Connections with Web Angles presented by Faella et al. [15].

Recently, a bolted-angle model was developed by Kim et al. [14] to simulate a top and seat angle connections with double web angles. This study presents a mechanical model using a component-based method where the stress-deformation relationships were obtained by analytical models. The method is a practical method for modeling the complex behavior of connections without much computational time required when compared with that of the detailed finite element models. The developed mechanical model considers key deformation components including the nonlinear behavior of the angles, the contact and detachment between the face of the column flange and connecting angles, and the column panel zone. The components are modeled by using one-dimension springs and are formulated in the force-displacement relationship. The details of this model will be discussed in the next chapter.

2.6 Cyclic testing of Braces and Buckling-restrained Braces

In this study, two different types of braces, regular buckling braces and buckling restrained braces (BRBs) were considered. This section presents the review of some relevant experimental results of both brace types under reversed cyclic loading. Summary of key test results to date is provided herein.

2.6.1 Cyclic Testing of Buckling Braces

KBMFs utilizes slender and stocky knee braces to dissipate seismic energy. Srechai et al.[22] conducted an experimental study on cyclic testing of knee braces. The specimens consisted of slender and stocky braces for comparison. The properties of the selected specimens are shown the Table 2.3.

Table 2.3 Properties of Selected Braces Tested under Cyclic Load [22].

Type	Section	Member Size	L/r	b/t
Slender Braces	angle	L25x25x3	133.87	8.3
Stocky Braces	square tube	75x75x4.5	22.81	16.7

Figures 2.24 and 2.25 show examples of the hysteretic response of the braces. The load and displacement values, normalized by the theoretical values of the yield load, P_y , and the yield displacement, Δ_y , are used to represent the response.

The result for the slender brace (Figure 2.24) showed that the compressive strength of the brace in the first cycle was smaller than the tensile strength due to buckling as expected. After buckling, as the applied displacement increased, the lateral deformation due to buckling intensified. The compressive strength of the brace was slowly reduced after each loading cycle. Finally, a plastic hinge formed at the center of the member which the axial strength of the member remained almost constant. The brace could sustain a very large ductility demand although with strength loss and very little energy dissipation as can be observed from the hysteretic loops. On the other hand, the stocky braces showed a large different hysteretic response. The response was stable with excellent energy dissipation as shown in Figure 2.25. The response shows stable hysteretic loops with little pinching behavior. The reduction in post buckling strength prior to local buckling was also small and the compressive strength of the specimens were still very close to the yield strength of the brace in tension.

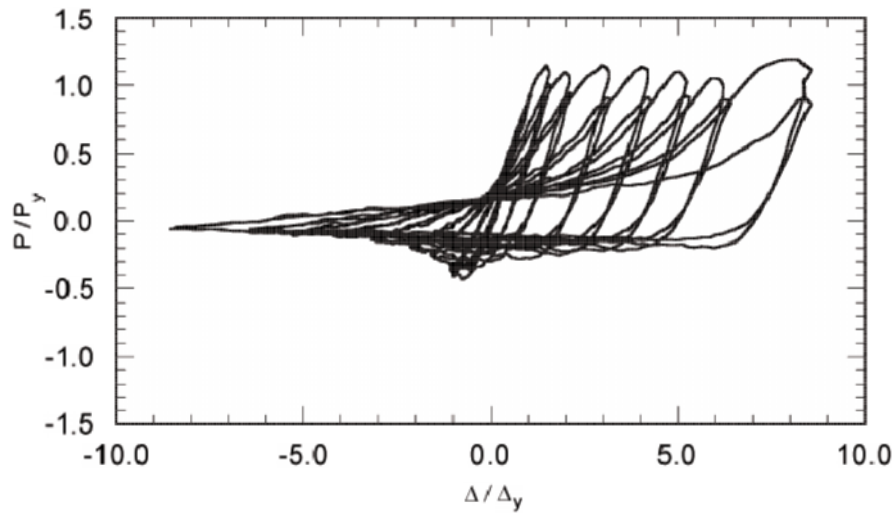


Figure 2.24 Hysteretic Response of Slender Brace (Angle Section) carried out by Serchai et al. [22].

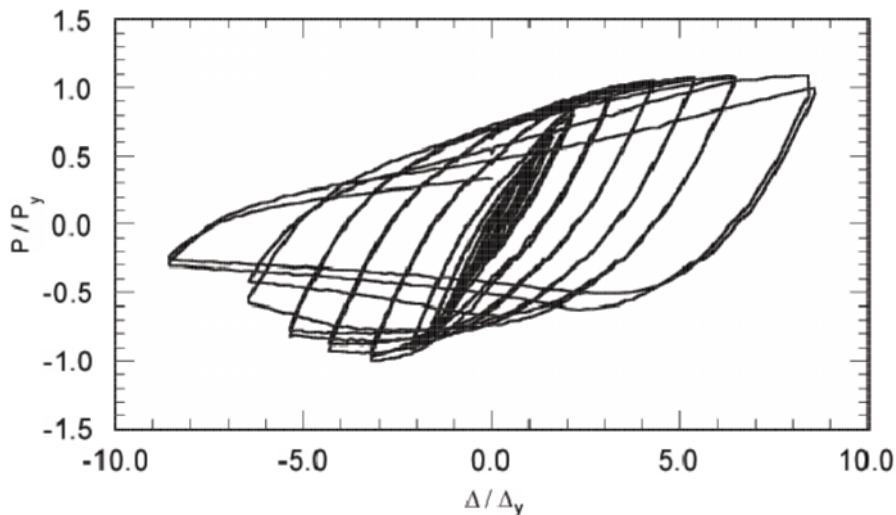


Figure 2.25 Hysteretic Response of Stocky Brace (Square Tube Section) carried out by Serchai et al. [22].

2.6.2 Cyclic Testing of Buckling-Restrained Braces

Buckling-restrained braces (BRBs) are one type of braces that provide large ductility capacity. BRBs generally comprise of a steel core element that carries the entire axial load and a restraining exterior element that prevents the core from buckling in compression. For this reason, a BRB yields in both tension and compression with out degradation of the brace capacity under compressive site. The concept of BRBs and the example of the hysteretic loop of BRBs are illustrated in Figure 2.26.

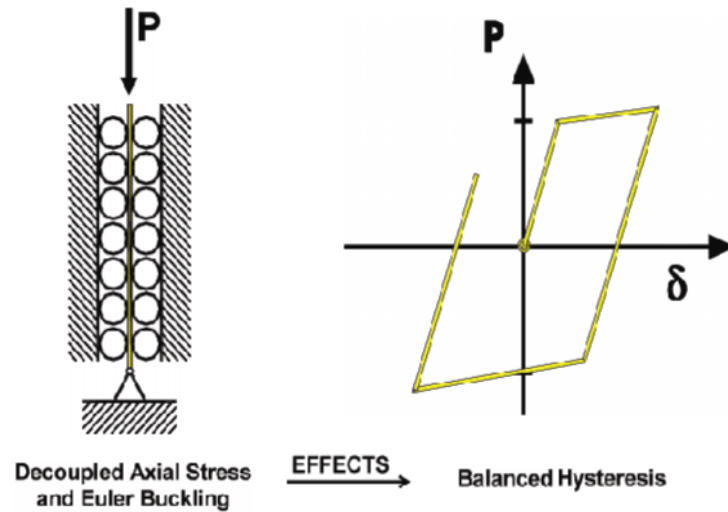


Figure 2.26 Mechanics of Buckling-Restrained Brace presented by Lopez and Sabelli [23].

The first strength and ductility of a BRB depend on the cross section areas and lengths of each part of the core. After yielding, BRBs strength increase in tension due to strain-hardening. In compression, the brace yields at the compressive yield strength while the lateral and local buckling behaviors are restrained by a restraining exterior element. Plastic hinges associated with buckling of slender braces do not form in properly designed and detailed BRBs. This behavior solves the problem of the braces buckle of that reduces the ductility of braces. The BRBs provide very good energy dissipation during earthquakes. The hysteretic behavior of conventional braces compares buckling-restrained braces are shown in Figure 2.27

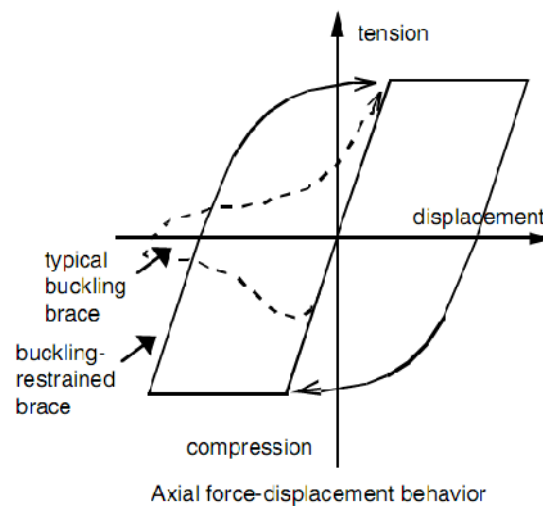


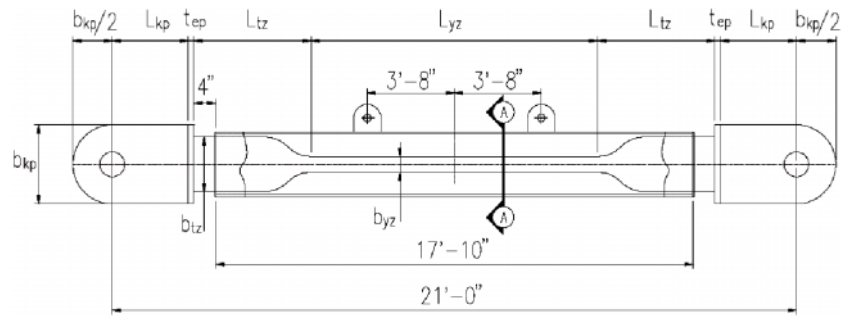
Figure 2.27 Behavior of Conventional Braces Versus Buckling-Restrained Braces [23].

Numerous BRB tests have been conducted and fully described herein. Table 2.4 shows the list of only those BRB concepts tested in support of actual U.S. building projects [23]. In the figure, ASTM refers to the American Society for Testing and Materials, and JIS refers to Japanese Industrial Standards.

Table 2.4 BRB Tests Summary by Lopez and Sabelli [23].

Literature Reference	Test Type	Number of Tested	Core Material	Length (ft)	Max. Strain (%)
SIE, 1999	Uniaxial	3	JIS G3136 SM 490A	14.75	2.07
				14.75	2.07
				14.75	2.07
SIE, 2001	Uniaxial	2	JIS G3136 SN 400B	14.75	2.07
				14.75	2.07
UC Berkeley, 2002	Frame (Subassemblage)	3	JIS G3136 SN 400B	9.83	2.12
				15.5	1.88
				15.5	1.81
Merritt et al., 2003a	Subassemblage	6	ASTM A36	18	2.50
				18	2.50
				18	2.68
				18	2.62
				18	2.48
				19	2.40
Merritt et al., 2003b	Subassemblage	8	ASTM A36	21	2.43
				21	2.48
				21	1.84
				21	2.47
				21	2.64
				21	2.54
				21	1.84
				21	1.77
Merritt et al., 2003c	Uniaxial	2	ASTM A36	20	1.60
				20	1.72
SIE, 2003	Subassemblage	4	JIS G3136 SN 400B	13.85	2.73
				24.78	1.64
				13.85	2.96
				24.78	1.63

In one series of tests, experimental study of eight full-scale buckling-restrained braces for Star Seismic was conducted by Merritt et al. [12] using a shake table facility at the University of California, San Diego. The specimens featured an A36 steel yielding element with concrete infill in a hollow structural section (HSS) casing. All of the specimens were tested under the standard loading protocol. The specimen dimensions and overview of the test set-up are illustrated in Figures 2.28 and 2.29, respectively.



(a) Member Core Geometry

Specimen	Steel Core plates					
	No. of plates	t_{ep} (in)	Transition Zone		Yielding Zone	
			b_{tz} (in)	L_{tz} (in)	b_{yz} (in)	L_{yz} (in)
1	2	0.75	10	23.00	2.53	176.0
2	2	0.75	10	21.28	3.97	179.4
3	2	0.75	10	19.36	5.56	183.3
4	2	1.00	10	18.44	6.33	185.1
5	4	0.75	10	18.89	5.95	184.2
6	6	0.75	10	21.28	3.97	179.4
7	6	0.75	10	18.41	6.34	185.2
8	8	0.75	10	20.33	4.77	181.3

(b) HSS and Collar Configurations

Specimen	HSS Configuration	Collar Plate Size
1	one-12×10× $\frac{3}{8}$ "	$\frac{3}{8}$ ×36" long
2	one-12×10× $\frac{3}{8}$ "	$\frac{3}{8}$ ×36" long
3	one-12×10× $\frac{3}{8}$ "	$\frac{3}{8}$ ×36" long
4	one-12×0× $\frac{3}{8}$ "	$\frac{1}{2}$ ×48" long
5	two-12×8× $\frac{1}{2}$ "	$\frac{1}{2}$ ×48" long
6	two-12×8× $\frac{1}{2}$ ", 1-12×12× $\frac{1}{2}$ "	$\frac{5}{8}$ ×60" long
7	two-12×8× $\frac{1}{2}$ ", 1-12×12× $\frac{1}{2}$ "	$\frac{3}{4}$ ×60" long
8	four-12×8× $\frac{1}{2}$ "	$\frac{3}{4}$ ×60" long

(c) Member End Geometry

Specimen	Knife Plate			End Plate
	t_{kp} (in)	b_{kp} (in)	L_{kp} (in)	t_{ep} (in)
1	1.5	14.5	14.0	1.0
2	1.5	14.5	14.0	1.0
3	1.5	14.5	13.0	2.0
4	1.5	14.5	13.0	2.0
5	1.5	18.5	12.0	3.0
6	1.5	22.0	12.0	3.0
7	1.5	22.0	12.0	3.0
8	1.5	22.0	12.0	3.0

Figure 2.28 Specimen Dimensions as summarized by Merritt et al. [12].

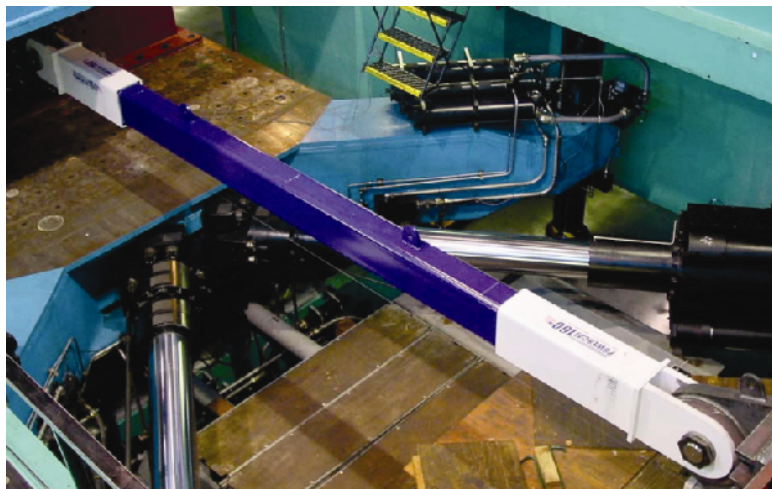


Figure 2.29 Overview of Example BRB Test carried out by Merritt et al. [12].

Specimen no.2 is chosen to show an example of the hysteretic response. The experimental results indicated that BRBs exhibited stable hysteresis loops with excellent ductility, stiffness, and energy dissipation as shown in Figure 2.30. The result shows that the BRB can reach yield strength in both tension and compression. The hysteretic response of BRBs is different from that of the traditional braces (Figure 2.24 and Figure 2.25).

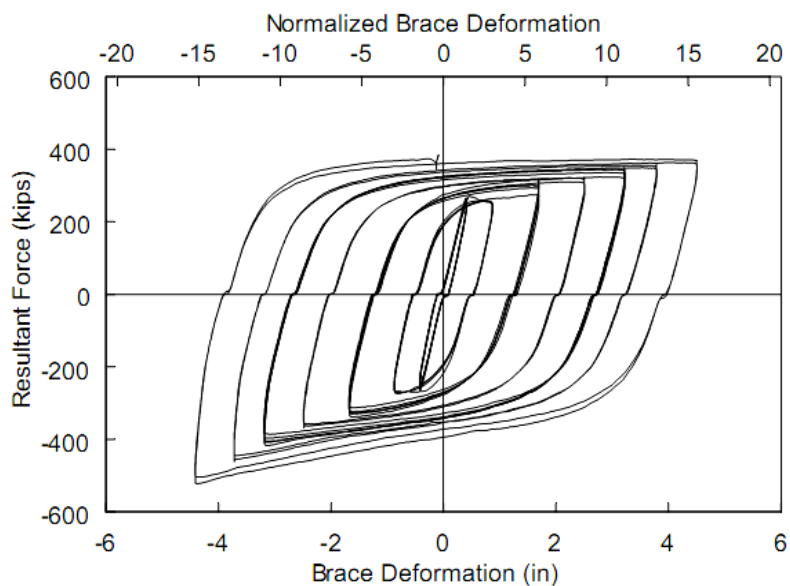


Figure 2.30 Hysteretic Response of BRB obtained by Merritt et al. [12].